nature photonics

REVIEW ARTICLE

PUBLISHED ONLINE: 31 MARCH 2010 | DOI: 10.1038/NPHOTON.2010.72

Optomechanical device actuation through the optical gradient force

Dries Van Thourhout* and Joris Roels

Optical forces are widely used to manipulate microparticles such as living cells, DNA and bacteria. The forces used in these 'optical tweezers' originate from the strongly varying electromagnetic field in the focus of a high-power laser beam. This field gradient polarizes the particle, causing the positively and negatively charged sides of the dipole to experience slightly different forces. It was recently realized that the strong field gradient in the near-field of guided wave structures can also be exploited for actuating optomechanical devices, and initial theoretical work in this area was followed rapidly by several experimental demonstrations. This Review summarizes the rapid development in this field. First, the origin of the optical gradient force is discussed in detail. Several experimental demonstrations and approaches for enhancing the strength of the effect are then discussed. Finally, some of the possible applications of the effect are reviewed.

Back in the 16th century, Johannes Kepler suggested that mechanical effects from solar radiation cause comet tails to point away from the sun. Today, optical forces are widely used to precisely control or measure the position of micrometre- to nanometre-sized particles[1]. Two major categories of optical forces are generally discerned: scattering forces and the gradient or dipole optical force. The scattering force can be regarded as a consequence of the momentum transfer from the radiating field to the dielectric medium, and is an axial force. It has been investigated in detail in the field of cavity optomechanics, first in large-scale Fabry–Pérot interferometers used for gravitational wave excitation[2], but more recently in the improvement of microfabrication technologies and also extensively in microscale structures[3,4] and on-chip microtoroids[3,4], in which the cavity field depends on the mechanical motion, and vice versa. Owing to the finite cavity decay time, this dependency gives rise to a 'dynamical back-action effect', as it was first coined by Braginsky[2]. In particular, the regime in which the photon lifetime exceeds the period of the mechanical oscillations has recently attracted significant attention as it allows the amplification[4,5] or dampening (cooling)[6–8] of mechanical oscillations through photon–phonon coupling. Ultimately this coupling should allow the observation of quantum mechanical behaviour in micromechanical resonators. Excellent reviews covering this domain have recently been published[9–11], and therefore the scattering force is not covered further in this Review. The gradient optical force, on the other hand, forms the basis of most optical tweezer set-ups and is related to strong variations in the electromagnetic field. Although it was already known that small particles can be trapped in the evanescent field close to dielectric interfaces[12–14], it was only recently proposed that the strongly enhanced gradient of the optical field close to nanophotonic waveguides could lead to significant optical forces, resulting in nanometre- or even micrometer-level displacements using milliwatt input power levels[15–17]. To understand the origin of the gradient force it is useful to first consider what happens when a polarizable microparticle is placed in a laterally varying optical field. It is well-known that in such cases a dipole will be induced in the particle, and the positively and negatively charged side of the dipole will experience slightly different forces in the gradient field. The particle will consequently be accelerated towards the region with the strongest field. This is the basic operating principle of optical tweezers, which trap microparticles in the waist of a powerful laser beam. Macroscopic structures such as integrated optical waveguides or resonators can be considered as a collection of individual microscopic dipolar subunits[18], and consequently can also be accelerated in a strongly varying electromagnetic field, such as the evanescent field in the region of a second waveguide. Compared with scattering forces, gradient forces can provide a much larger force per photon when strong field gradients are available. The optical gradient force may therefore be an alternative actuation force for micro-electromechanical systems, and may enable the realization of micro-optomechanical systems.

To get a feeling for the nature of the optical gradient force, consider the simple configurations shown in Fig. 1a. A dielectric strip waveguide, which can freely move (with spring constant k), is placed in the evanescent field of an eigenmode propagating in a second waveguide. To calculate the power exerted by this field on the free-hanging waveguide, one can make use of the Maxwell stress tensor formalism[18]. From Maxwell's equations and the Lorentz' force law, which connects mechanical motion to electromagnetic fields, it is straightforward to derive that the time-averaged force

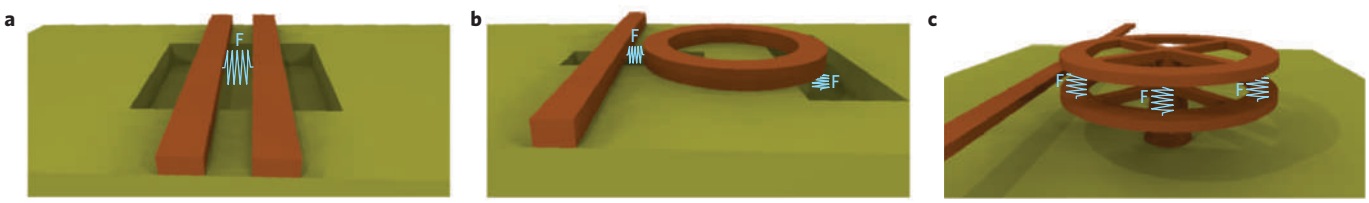

Figure 1 | The optical gradient force acting on integrated waveguide structures. a, The force between two parallel waveguides. **b**, Force enhancement through the use of an integrated resonator. **c**, Coupled resonator configuration.

Department of Information Technology, Ghent University-IMEC, St. Pietersnieuwstraat 41, 9000 Gent, Belgium. *e-mail: dries.vanthourhout@ugent.be

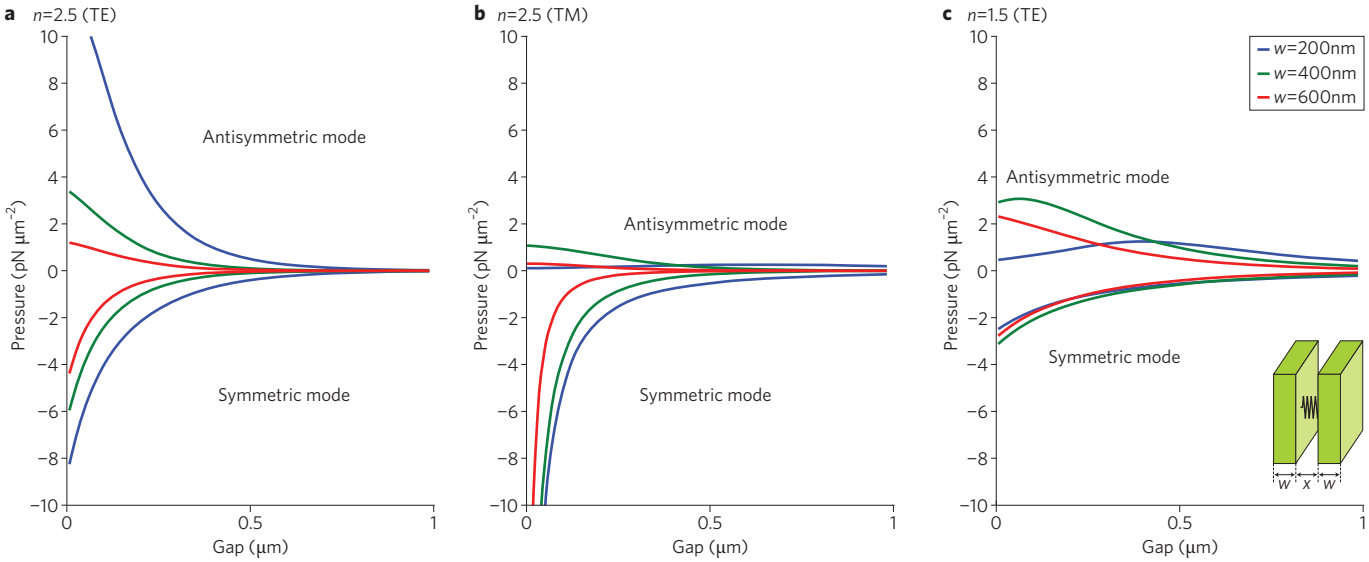

Figure 2 | The pressure between two slab waveguides excited with a symmetric (attractive) or antisymmetric (repulsive) mode as function of their separation. Excitation was achieved at an input power of 1 mW μm^{-1}, and slab waveguide thicknesses of 200, 400 and 600 nm were used. **a**,**b**, Results achieved with a slab waveguide refractive index of n = 2.5. **c**, Results achieved with a slab waveguide refractive index of n = 1.5. The electromagnetic field is transverse electric (TE) polarized in **a** and **c**, and transverse magnetic (TM) polarized in **b**.

exerted on a rigid body within a closed volume V can be calculated from the surface integral $\langle F\rangle = \int_{\partial V}\langle\overline{\mathrm{T}}(\boldsymbol{r}, t)\rangle\cdot\mathrm{n}(\boldsymbol{r})ds$, where $\overline{\mathrm{T}}(\boldsymbol{r}, t)$ is the Maxwell stress tensor whose components are given by $T_{ij} = \varepsilon\varepsilon_0(E_iE_j - \delta_{ij}\boldsymbol{E}^2/2) + (B_iB_j - \delta_{ij}\boldsymbol{B}^2/2)/\mu\mu_0$. Here, δ_{ij} is the Kronecker delta, E_i and E_j are components of the electric field $\boldsymbol{E}$, B_i and B_j are the components of the magnetic induction $\boldsymbol{B}$, ε and μ respectively denote the dielectric constant and magnetic susceptibility of the medium surrounding the rigid body, and ε_0 and μ_0 respectively denote the permittivity and permeability of free space. Note that the enclosing surface ∂V can be arbitrarily chosen, which allows the fields to be evaluated at the surface of the body as well as in the far-field. Both the scattering and the gradient force can be obtained from this calculation.

This method, however, does not provide significant physical insight. One can alternatively derive the force from the change in the eigenmode frequency ω of the waveguide system when the two beams move towards each other, which causes a change in the total energy of the system. By arguing that the work done by the beam, Fdx, should equal the change in energy, dU, Povinelli *et al.*[16] derived that the mechanical force can also be calculated as

$$F = -\frac{1}{\omega}\frac{d\omega}{dx}\bigg|_{\boldsymbol{k}} U \qquad (1)$$

where x is the distance between the beams, U is the total system energy and $\boldsymbol{k}$ is the wave vector, which is conserved.

Several authors have verified that equation (1) is indeed equivalent to the Maxwell stress tensor formalism[16,19,20]. A frequency decrease leads to a lowering of the system energy, and hence induces an attractive force. From this equation, it is also immediately obvious that the optical force is proportional both to U and the optomechanical coupling coefficient, defined as $g_{\mathrm{om}} \equiv d\omega/dx$. To get a better understanding of the meaning of this parameter, consider what happens when two identical waveguides are brought together. In general their eigenmodes will couple and the degeneracy will be removed. Symmetric (bonding) and antisymmetric (antibonding) modes can form, with eigenfrequencies of either $\omega_+ = \omega_0 - \Delta\omega_+(x)$ or $\omega_- = \omega_0 + \Delta\omega_-(x)$, respectively, where x is the gap between waveguides. The quantity $\Delta\omega_\pm(x)$ can be calculated using first-order perturbation theory[21] and depends on the strength of the field of the first waveguide at the location of the second waveguide. This overlap is largely determined by the distance between both cavities, and decreases exponentially with increasing x. However, other parameters such as the refractive index and the waveguide dimensions also determine the strength of the coupling. This is shown in Fig. 2, which shows the optical force for a configuration consisting of two slab waveguides with refractive index n, thickness w and separation x, using equation (1). A similar configuration was studied by Riboli *et al.*[22] using the Maxwell stress tensor formalism. Figure 2a, with n = 2.5 and a transverse electric polarization (electric field in the plane of the slab), shows that the optomechanical interaction indeed increases exponentially for decreasing waveguide separation. It also shows that the force is negative (attractive) for the symmetric mode, and positive (repulsive) for the antisymmetric mode. For the transverse electric polarization the attractive and repulsive forces are almost in equilibrium. However, for transverse magnetic polarization, the attractive force can be much stronger than the repulsive force (Fig. 2b). This can be explained by the strong enhancement of the orthogonal electric field component in the gap — an affect well-known in slot-waveguide theory[23,24] — which is a direct consequence of the electromagnetic boundary conditions. If the refractive index of the slab is decreased (Fig. 2c), for small separations the forces are now smaller than in the high refractive index case. However, for longer distances the force becomes larger than for the high refractive index case, as the exponential decay is governed by the refractive index contrast, given by

$$g_{\mathrm{om}} = \exp\left(\frac{-2\pi x\sqrt{n_{\mathrm{eff}}^2 - 1}}{\lambda_0}\right)$$

where λ_0 is the vacuum wavelength and n_{eff} is the effective mode index. Increasing the refractive index to n = 3.5, for example, would enhance the forces at small gap distances, compared with those of Fig. 2a. Figure 2c also shows that the force is not always a monotonous function of the gap distance: for small waveguide widths the repulsive force reaches a maximum and then decreases again as the separation approaches zero. This phenomenon is related to the low optical field confinement in thinner waveguides. Povinelli *et al.*[16]

showed that, when considering two silicon strip waveguides, owing to edge effects at the top and bottom of the strip waveguide, the optical force can even change sign for small gap distances. The authors also predicted that, for two beams with a length of 30 μm, a cross-section of 310 nm × 310 nm and an input power of 100 mW, a deflection of 20 nm could be expected. Equation (1) is in principle a closed-system description; Rakich *et al.*[19] recently derived a more general formalism that is valid for open systems, with an optical response that can be altered through a single mechanical degree of freedom. They demonstrated that the optical force (or an equivalent optical potential) is fully determined by the frequency-dependent scattering matrix of the optical system, thereby providing a very powerful tool for synthesising an optical system with complex optical force profiles.

In 2008, Li *et al.*[25] experimentally demonstrated the optical gradient force using a variation of the configuration first theoretically introduced by Povinelli *et al.*[16]: light was injected into a silicon strip waveguide[26] that was under-etched over a distance of 10 μm to create a free-hanging beam, with the evanescent tail of the field in the beam leaking into the underlying SiO_2 slab. In this particular case, decreasing the gap increased the refractive index — which corresponds to a frequency decrease — thus allowing only attractive forces to be demonstrated. This was overcome in later work by Li *et al.*[27] and Roels *et al.*[28], which utilized two parallel silicon strip waveguides with cross-sections of 220 nm × 500 nm (Fig. 4a). The integration of an asymmetric Mach–Zehnder interferometer in front of the coupler allows controllable excitation of either the bonding or the antibonding mode by scanning the pump wavelength. Depending on the wavelength, the relative phase between the two outputs of the Mach–Zehnder interferometer can be varied from 0 to 2π. If both modes are in phase (antiphase), the symmetric (asymmetric) mode of the coupler is excited, resulting in an attractive (repulsive) force. Any linear combination of these two modes causes the optical force to vary between both extrema. Attractive forces of the order of 0.2 pN μm^{-1} mW^{-1} and repulsive forces of the order of 0.1 pN μm^{-1} mW^{-1} were measured by Roels *et al.*[28] (Fig. 3c). When both the bonding and antimode are excited simultaneously, the forces do not only add incoherently — a beating term must also be taken into account[27].

The experimental procedure in this work[27,28], outlined in Fig. 3, is exemplary for most of the experiments described in this Review. A pump beam at wavelength λ_1 induces a mechanical displacement dx, which is then probed through a second beam at wavelength λ_2. The transduction mechanism, which translates the mechanical movement into an amplitude modulation $T(\lambda_2)$ of the probe beam, is typically provided by the optical structure itself, for example, by inserting it in a cavity or in one of the arms of an interferometer. The mechanical response of the beam is governed by the equation of motion:

$$m\ddot{x} + \gamma\dot{x} + kx = F_{\mathrm{opt}}(x) + F_{\mathrm{Brown}} \qquad (2)$$

where m is the effective mass of the beam, γ is the beam damping constant, k is the spring constant, $F_{\mathrm{opt}}(x)$ is the gap-dependent optical dipole force and F_{Brown} is the thermal displacement (Brownian) noise. Under static operation the beam displacement is then $\Delta x = F_{\mathrm{opt}}/k = g_{\mathrm{om}}U/k\omega_0$, which is strongly dependent on the spring constant. To overcome the stiffness of the mechanical structure, the pump beam is often modulated at the resonance frequency of the beam,

$$\Omega_{\mathrm{m}} = \sqrt{\frac{k}{m}}$$

which results in an enhancement to the displacement amplitude that is proportional to the mechanical quality factor of the structure, given by $Q_{\mathrm{m}} = \Omega_{\mathrm{m}} m\gamma^{-1}$.

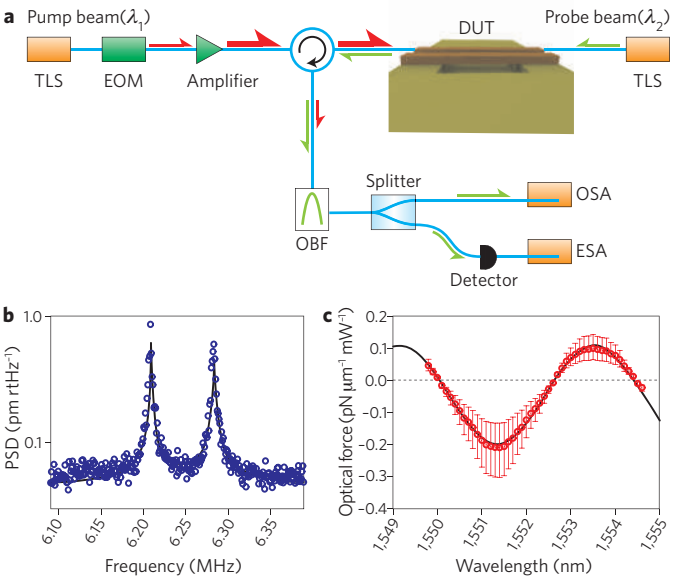

Figure 3 | Measurement and calibration procedure. a, Typical experimental set-up. TLS, tunable laser source; EOM, electro-optic modulator; DUT, device under test; OBF, optical bandpass filter; OSA, optical spectrum analyser; ESA, electrical spectrum analyser. **b**, Calibration using beam thermal noise. PSD, power spectral density. **c**, Attractive and repulsive optical forces in a two-beam experiment. Error bars are the estimated error in the actual optical power inside the device. Figure **c** reproduced from ref. 28, © 2009 NPG.

Resonator-enhanced gradient force

Equation (1) shows that the dipole force scales with the energy in a nanostructure, and hence it is unsurprising that several attempts have been made to increase the effect of the optical forces by using resonant structures. In this section, structures consisting of a single resonator coupled to an access waveguide are outlined (Fig. 1b). The time-dependent evolution of the amplitude a in an optical resonator is in general described by[9,31,32]:

$$\frac{da}{dt} = \left(j\omega_0(x) - \frac{1}{2\tau_0(x)} - \frac{1}{2\tau_{\mathrm{ext}}(x)}\right)a + j\sqrt{\frac{2}{\tau_{\mathrm{ext}}(x)}}\,s \qquad (3)$$

where $\omega_0(x)$ is the resonance frequency of the cavity, $\tau_0(x)$ is the intrinsic lifetime of the cavity and $\tau_{\mathrm{ext}}(x)$ is the external decay rate. The energy stored in the cavity is given by $U = a.a^*$, and the input power to the resonator is given by $P_{\mathrm{in}} = s.s^*$. Each of the parameters in equation (3) may be dependent on the displacement x of the mechanical structure coupled with the cavity; changes in the gap will therefore affect the evolution of the resonating field. In most of the structures described in this Review, we assume that the variation of the mechanical displacement is slow compared with the cavity lifetime (that is, $\tau_0^{-1} >> \Omega_{\mathrm{m}}$), and that the circulating optical power responds adiabatically to changes in the optomechanical coupling. The only optical 'back-action' effect in this case is the so-called optical spring effect; because the strength of the optical force in equation (2) is dependent on the displacement coordinate, it can in some cases lead to a considerable virtual stiffening or softening of the structure, accompanied respectively by an increase or decrease of the mechanical resonance frequency. An example of this is given below.

Eichenfield *et al.*[33] studied a configuration in which the external decay rate $\tau_{\mathrm{ext}}(x)$ was strongly dependent on the displacement parameter x, while $\omega_0(x) = \omega_0$ was kept fixed. A SiN microdisk resonator with a high optical quality factor ($Q = 1.1 \times 10^6$) was coupled to a silica optical fibre taper (Fig. 4b). The taper was made

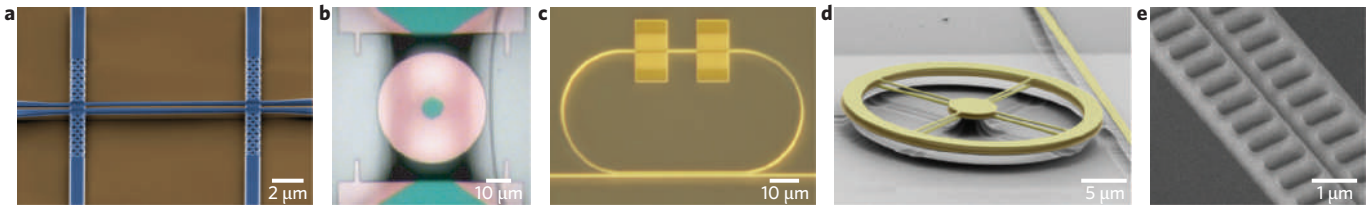

Figure 4 | Recent optomechanically driven nanostructures. a, Two parallel silicon strip waveguides. **b**, SiN_x microdisk coupled to a fibre taper. **c**, Silicon ring resonator with a photonic-crystal-supported nanomechanical beam. **d**, Vertically coupled SiN disk resonator. **e**, Laterally coupled ladder photonic crystal cavities. Figures reproduced with permission from: **a**, ref. 27, © 2009 NPG; **b**, ref. 33, © 2007 NPG; **c**, ref. 34, © 2009 OSA; **d**, ref. 40, © 2009 NPG; **e**, ref. 44, © 2009 NPG.

flexible to allow it to move towards the microdisk under the influence of the optical gradient force. Transmission through the fibre depended on its position relative to the microdisk: if the gap is large then almost no power will couple to the microdisk and the transmission at resonance will show only a small dip. When the fibre is moved closer, the coupling rate increases until it finally matches the cavity loss rate (critical coupling), where all the power is coupled to the microdisk. At this point the transmission falls to zero and the energy in the resonator is at its maximum. When moving further towards the microdisk, the resonator is over-coupled and the energy in the resonator starts to decrease again. One would expect the optical force to be maximal at the critical coupling point, where the energy in the resonator is maximal. However, the optical force is not only dependent on the optical power in the ring, but also increases exponentially with decreasing gap distance. As a result, the distance where the optical force is maximal occurs at a point closer to the disk than the critical coupling point, in the over-coupled regime. This also explains why the authors found the maximum optical force to be independent of the quality factor of the disk resonator[33]. If the quality factor increases, the power enhancement in the microdisk increases, but the distance between the microdisk and input waveguide where this enhancement occurs also increases. Reducing the size of the cavity, however, does increase the optical force. The spring constant of the optical fibre taper used as the input coupler is rather low (38 pN μm^{-1}), which has allowed experiments to use low-power CW signals to measure very large displacements (>100 nm). The researchers demonstrated switching of a probe signal with an extinction ratio of 21 dB using a 0.9-mW pump beam[33].

Pernice *et al.*[34] studied an alternative configuration, in which the external coupling rate was kept constant but the resonance frequency $\omega_0(x)$ was made gap-dependent by partly under-etching a silicon microdisk resonator in a manner similar to their previous work[25]. The now free-hanging beam (length 10 μm, Q_m = 1,200) is purely dispersively coupled with the underlying substrate: when it moves towards the SiO_2 slab the resonance frequency shifts but the resonance linewidth is unaffected — in this case, therefore, increasing the optical quality factor increases the sensitivity. The shift in resonance frequency can thus be used to measure the displacement of the beam directly. Pernice *et al.*[34] measured a single-sided displacement sensitivity of $\sqrt{S_x}$ = 40 fm/$\sqrt{\text{Hz}}$, in this case limited by the relatively low optical quality factor (Q = 4,200) and the relatively low optomechanical coupling factor. Anetsberger[35] demonstrated a hybrid version of this structure in which the optical resonator and the mechanical resonator were fabricated separately and brought together using piezoelectric actuators. This set-up has the advantage that the optical resonator, a toroid silica microcavity with a radius of 58 μm and an optical quality factor of $Q = 7.8 \times 10^7$ (a finesse of 230,000), and the mechanical resonator, SiN doubly clamped strings with mechanical quality factors of 10^4–10^5 and fundamental resonance frequencies of 6.5–16 MHz, can be optimized separately. An optomechanical coupling rate of up to 20 MHz nm^{-1} was experimentally demonstrated[35]. Using this configuration, a room-temperature single-sided displacement sensitivity of $\sqrt{S_x}$ = 640 fm/$\sqrt{\text{Hz}}$ was derived from the background measurement. By using smaller microcavities and shorter wavelengths, further improvements are expected. An improvement of at least one order of magnitude to the mechanical quality factor of the SiN strings should be possible without compromising the resonance frequency[36]. Owing to the high optical quality factor of the silica microtoroid, in this configuration the photon lifetime exceeds the mechanical oscillation period and the optical field is no longer able to follow the mechanical displacements adiabatically, thereby giving access to the 'resolved sideband regime'[9]. As discussed earlier, either amplification or dampening of the oscillations is possible in this regime. By using a pump laser blue-shifted with respect to the optical cavity resonance frequency, the authors were able to amplify the oscillations of the SiN string, as well as observe clear threshold behaviour and a strong narrowing of the mechanical linewidth. The mechanical oscillations also led to amplitude modulation of the pump beam, in this case with a near-unity extinction ratio. The resulting radiofrequency signal could therefore serve as an optical clock, with a linewidth that is limited by thermal noise. Although this particular structure used by Pernice *et al.*[34] exploited external actuators to bring the microtoroid and SiN membrane together, one could envisage that, if the optical quality factor of the silicon ring resonator was sufficiently increased, the results could lead to extremely compact fully integrated all-optical clocks.

Resonator–resonator coupling

It has been known for a long time that two microparticles in the presence of a plane wave or near a dielectric surface can show bonding behaviour[12,13]. In 2005 it was theoretically proposed that this behaviour could be greatly enhanced by exploiting the whispering-gallery modes (or morphology-dependent resonances) of glass microspheres[15,37]. It was shown that the optical force in such a configuration is enhanced in proportion to the optical quality factor of the resonator. Forces of up to 100 nN were predicted for microspheres with a quality factor of $Q = 10^8$, with corresponding displacements of over 1 μm when these spheres are attached to a fibre stem with a spring constant of k = 0.004 N m^{-1} (ref. 15). Later, Ward[38] proposed a method to control the relative positions of two such microspheres using two pump beams that individually control the strength of the attractive and the repulsive forces. In this way an optical potential profile can be generated, which binds the microspheres to a given location. In 2006 Notomi *et al.*[17] proposed the vertical coupling of two planar photonic crystal cavities. Although the optical quality factor of the considered cavities was at least two orders of magnitude lower than of the double-microsphere configuration, the predicted normalized force was up to three orders of magnitude larger for the double-layer photonic crystal cavity. This can be understood by considering the greatly enhanced relative field overlap of both cavities, expressed through the optomechanical coupling factor g_{om} of the structure. It was

also predicted that if the cavity distance could be changed within the photon lifetime, adiabatic tuning of the wavelength over more than 100 nm should result. Rakich *et al.*[39] considered the case of two vertically coupled ring resonators, and in particular investigated the optomechanical potential formed by the resonances originating from neighbouring modes, which cross when the distance between the rings decreases. In this case a single pump beam allows a potential to be created, trapping the structure in a well-defined position.

Similar to the case of two simple waveguides as discussed above, when two identical optical resonators are brought close together, bonding and antibonding modes will both form. The stronger the coupling between the cavities, the further their respective eigenfrequencies will be pushed away from each other and the stronger the associated force will become. Again, the coupling is strongly dependent on the distance between both cavities but is also dependent on the particular configuration. For example, in the case of the microsphere resonators discussed above[15,37], there is only a 'point contact' between both resonators, whereas for the vertically coupled ring resonators[30,40] (Fig. 1c) and in particular for the vertically coupled photonic crystal cavity[17], the overlap extends over the full cavity, resulting in a much larger optomechanical coupling factor.

The vertically coupled disk resonator configuration has been experimentally investigated both by Rosenberg *et al.*[30,41] and by Wiederhecker *et al.*[40]. Rosenberg *et al.* used 400-nm-thick, 54-μm-radius SiO_2 disks separated by 150 nm and with optical quality factors of ~1×10^6. In contrast, Wiederhecker *et al.* used 190-nm-thick, 30-μm-radius SiN_x disks separated by 1,050 nm and with optical quality factors of ~8×10^4. In both cases, spokes were introduced to the centre of the disks to reduce the mechanical stiffness of the structure to ~1–10 N m^{-1} (ref. 3). As a result, in both cases considerable deflection (~10 nm) was measured even under static operation. The much smaller gap in the work of Rosenberg *et al.*, however, resulted in a much larger optical coupling factor (g_{om} = 31 GHz nm^{-1}). Resonance tuning by more than 4 nm was demonstrated, achieved using a pump power of only 1.5 mW — equivalent to a tuning power of 309 GHz mW^{-1} (Fig. 5a). An on–off switching time of 200 ns was demonstrated, which could be further reduced to 7 ns by exploiting the transduction gain. For comparison, so far some of the best results for the thermo-optic tuning of silicon structures efficiencies almost an order of magnitude lower, and much longer switching times[42,43]. One drawback of the low spring constant for these structures is their sensitivity to thermal fluctuations. At low input powers, strong fluctuations of the power are observed. However, as discussed above, because the circulating optical energy is gap-dependent, the optical gradient force introduces a dynamical back-action and therefore influences the mechanical properties of the structure. From equations (2) and (3) one can derive that an effective optical string constant is introduced, which depends on the wavelength detuning from the cavity resonance and is proportional to $g_{om}^2 P_i$, where P_i is the power injected in the cavity[9,30,44]. The impact of the optical spring effect is particularly strong in this case because of the low mechanical spring constant for the double-ring resonator structure. Figure 5b shows the probe modulation spectra for increasing pump powers. Using a similar structure — but without spokes — Lin *et al.* demonstrated regenerative mechanical oscillation and cooling[45]. Although the optical quality factor was not exceptionally high ($Q = 1.75 \times 10^6$), the very strong optomechanical coupling results in a threshold input power as low as 270 nW for the onset of regenerative mechanical oscillations (in vacuum), clearly showing the benefits of gradient optical force cavities in producing ultrastrong retarted dynamical back-action effects.

Eichenfield *et al.*[44] experimentally demonstrated two optomechanically coupled photonic crystal cavities. Contrary to the planar cavity proposed previously[17], this work uses a photonic crystal consisting of a one-dimensional pattern of holes etched in a SiN

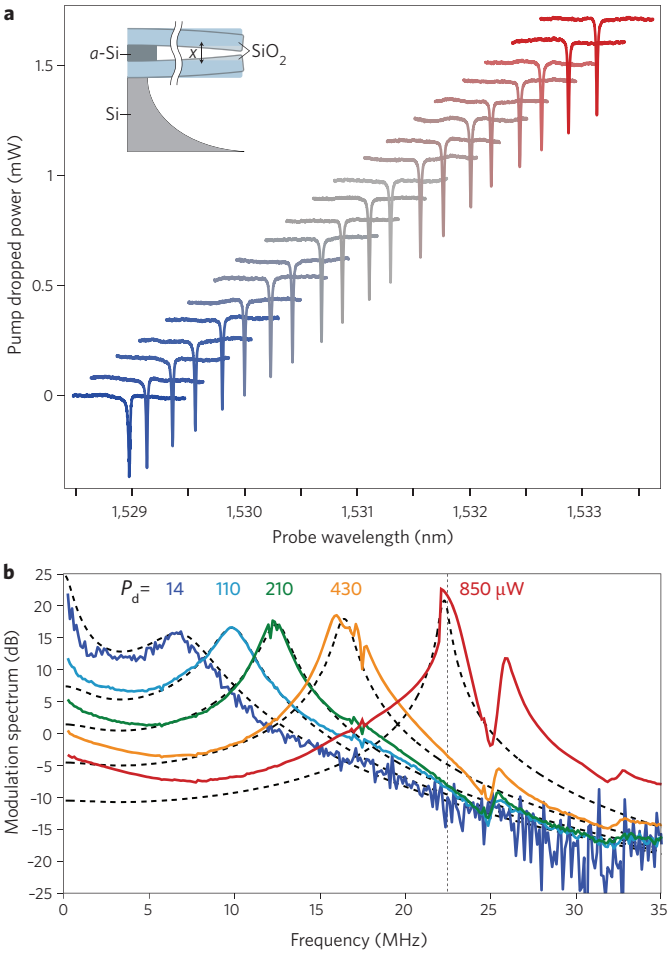

Figure 5 | Static and dynamic response of a double-disk resonator. **a**, Resonance wavelength tuning[30]. Inset, optical spring effect in a double-disk resonator. **b**, The optical spring effect induces a strong increase in mechanical resonance frequency when the pump power is increased. Figure reproduced from ref. 30, © 2009 NPG.

nanobeam (Fig. 4d). The lattice period is graded in such a way that localized modes form in the centre of the beam, with theoretical optical quality factors of more than 10^6, and experimental optical quality factors of around 10^5. A fibre taper was used for probing the modes of the resulting 'zipper' cavity. By moving the fibre taper laterally over the zipper cavity, the nature of the modes (symmetric or antisymmetric) could be identified. By scanning the frequency of the probe beam up to 150 MHz and linking the results to finite-element method simulations, a rich family of mechanical modes was identified; the combined cavity was found to exhibit both common and differential modes — beams moving the in same or opposite direction, respectively — and both in-plane and out-of-plane modes were detected. The mechanical quality factor for these modes, limited by the 1 atm gas environment, varied from 50 to 150. It should be possible, however, to increase the quality factor up to 1×10^4 if the experiments are performed in a vacuum[44]. A very large coupling constant of g_{om} = 123 GHz nm^{-1} was experimentally determined, which agrees with the values predicted in ref. 17 and is in line with the strong interaction between both cavities. Camacho *et al.*[46] performed a detailed analysis of the thermo-optic tuning and the thermo-mechanical tuning in the zipper cavity and found that they are indeed non-negligible.

Eichenfeld *et al.*[47] went one step further and demonstrated that a similar structure could function simultaneously both as a photonic and phononic crystal, thereby allowing the co-localization and strong

coupling of photons and phonons. This was expressed through the theoretically predicted and experimentally verified coupling length, given by

$$L_{om} = \left(\frac{1}{\nu_0}\frac{d\nu_0}{dx}\right)^{-1}$$

where ν_0 is the cavity response frequency, close to the limit of the wavelength of light (L_{om} = 2.9 μm, equivalent to g_{om} = 66 GHz nm^{-1}). The localized phononic modes exhibit very high mechanical resonance frequencies ranging from 850 MHz up to 2.25 GHz. Furthermore, because the mechanical modes are decoupled from their supports, they also exhibit a relatively high mechanical quality factor of Q_m = 1,300 in air, resulting in one of the highest-frequency quality factor products reported so far. An overview of the most relevant optomechanical structures (and their parameters) covered in this Review can be found in Table 1.

Discussion

Over the past five years, rapid progress has been made in understanding and experimentally demonstrating optomechanically actuated systems that exploit the gradient force. Through exploiting the evanescent field of guided wave structures, the gradient optical force allows for photon momentum to be exchanged[45] over a distance approaching the wavelength of the light[44,45,47]. This is in stark contrast with classical optomechanics[9,10], which relies on the scattering optical force. In classical optomechanics the effective coupling length $L_{om} = \omega_0/g_{om}$ is proportional to the cavity roundtrip length and is typically at least several tens of wavelengths. From first theoretical proposals the field now has rapidly moved forward to experimental demonstrations, and first applications may not be far off. Sensing — mass spectroscopy, force detection and charge sensing in particular — is a strong candidate for a practical application. Micromechanical structures such as cantilevers and doubly clamped beams are now already widely used for this purpose, and resolution down to the zeptogram scale has been demonstrated[48]. The major limitation of these structures is typically the motion-detection efficiency using electrical readout techniques. Optical readout techniques have therefore been proposed using either free-space optics[49] or guided wave optics[50]. However, these devices still require electrical actuation, which in many cases limits the operational bandwidth. This limitation could be overcome by using optical actuation, and any of the structures discussed above could be used to achieve this. By modulating the pump beam, the mechanical structure is actuated. The change in mechanical resonance frequency, resulting from a change in the mass of the beam, can then be read-out through the probe beam. In 2009, a structure consisting of two cantilevers in line, specifically designed for this purpose, was proposed[51]. Optical actuation of one of the cantilevers reduces the transmission between them and can directly be read-out as an amplitude modulation. Compared with the other structures discussed above, which rely on multiple-beam interference to translate a phase modulation into an amplitude modulation, this approach allows for the use of a cheap broadband source. Furthermore the optomechanical crystal used by Eichenfield *et al.*[47] shows significant promise for mass-sensing applications. Owing to the low effective mass (62 fg) of the mechanical mode and to the high mechanical resonance frequency (850 MHz), resolutions similar to those of zeptogram mass sensors[48] should be realistic.

Application as a building block in all-optical switch matrices or optically reconfigurable networks may also be a next step. Wavelength tuning based on the double-ring structure of Rosenberg *et al.*[30] (Fig. 5) now already outperforms thermo-optical tuned structures in terms of power consumption and speed. Other physical effects such as carrier injection[52] or depletion[53] may be more efficient or faster, but these have limited tuning range and induce losses, thereby compromising the optical quality factor. The latter is not the case for the optomechanical tuning process, which is purely dispersive. Using the techniques proposed in refs 19,38,39, complex optomechanical potential profiles can be built using single or multiple optical pump beams, thereby allowing precise control over the position of micromechanical structures. Wavelength conversion is another important function in all-optical networks. However, although this has been theoretically proposed[17], experimental confirmation has yet to be achieved.

On a more fundamental level, when the optical cavity lifetime approaches the mechanical oscillation period, new effects arise. Discussed above are the observations of coherent oscillations in a membrane-coupled microtoroid resonator[35] and in a double-disk resonator[45]. By detuning the pump wavelength to the red side of the optical resonance, optical cooling is also feasible[9,45]. This regime has not yet been reached for fully integrated photonic circuits,

Table 1 | Summary of the most relevant parameters for results discussed in text, highlighting the efforts being undertaken towards reaching higher optomechanical coupling coefficients and higher mechanical resonance frequencies.

Authors	Year	Structure	$\frac{g_{om}}{2\pi}$ (GHz nm^{-1})	Optical *Q*-factor	$\frac{\Omega_m}{2\pi}$ (MHz)	*k* (N m^{-1})	Mechanical *Q*-factor	F_{opt} (pN mW^{-1})	Δx (nm)
Li *et al.*[25]	2008	Single beam	~7*	—	8.87	3.6	1,850	5	2.5‡
Li *et al.*[27]	2009	Double beam	~2.8*	—	18	16.8	5,300	2	~2*,‡
Roels *et al.*[28]	2009	Double beam	~2.8*	—	5.8	—	6,000	4	—
Eichenfield *et al.*[33]	2007	SiN disk-fibre	—	1.1×10^6	193×10^{-6}	65×10^{-6}	—	20	120
Pernice *et al.*[34]	2009	Partly under-etched silicon ring	~0.4*	4,200	4.88	—	1,200	—	—
Anetsberger *et al.*[35]	2009	Toroid-SiN membrane	0.02	7.8×10^7	6.5–16	~8	10^4–10^5	—	1–10‡
Povinelli *et al.*[15]	2005	Double sphere	~0.2*	10^8	—	0.004	—	—	1,000‡
Rosenberg *et al.*[30]	2009	Double ring	31	10^6	~7	9.5	—	98,000*†	17.7
Wiederhecker *et al.*[40]	2009	Double ring SiN	1.25	8×10^4	10	2.3	15.8	12,000†	12
Eichenfield *et al.*[44]	2009	Coupled photonic crystal	123	10^4–10^5	~8	110	50–150	—	—
Eichenfield *et al.*[47]	2009	Optomechanical crystal	66	3.8×10^4	850–2,250	—	1,300	—	—

*Values were estimated from the data available within the reference. †Force normalized with respect to the pump drop power; the actual power in the cavity is strongly enhanced through the resonance effect. ‡Measured at the mechanical resonance frequency Ω_m.

which combine access waveguides and resonators on a common chip platform. However, from the results shown of refs 34,45, it is clear that it is only a matter of time before this is achieved. Such circuits will open the path towards coupling multiple mechanical and/or optical resonators[54,55] and the full optical integration of, for example, optically driven clocks.

References

1. Chu, S. Laser manipulation of atoms and particles. *Science* **253,** 861–866 (1991).
2. Braginsky, V. B. & Manukin, A. B. *Measurement of Weak Forces in Physics Experiments* (Univ. Chicago Press, 1977).
3. Anetsberger, G., Rivière, R., Schliesser, A., Arcizet, O. & Kippenberg, T. J. Ultralow-dissipation optomechanical resonators on a chip. *Nature Photon.* **2,** 627–633 (2008).
4. Kippenberg, T. J., Rokhsari, H., Carmon, T., Scherer, A. & Vahala, K. J. Analysis of radiation-pressure induced mechanical oscillation of an optical microcavity. *Phys. Rev. Lett.* **95,** 033901 (2005).
5. Braginsky, V. B., Strigin, S. E. & Vyatchanin, S. P. Parametric oscillatory instability in Fabry–Pérot interferometer. *Phys. Lett. A* **287,** 331–338 (2001).
6. Arcizet, O., Cohadon, P.-F., Briant, T., Pinard, M. & Heidmann, A. Radiation-pressure cooling and optomechanical instability of a micromirror. *Nature* **444,** 71–74 (2006).
7. Gigan, S. *et al.* Self-cooling of a micromirror by radiation pressure. *Nature* **444,** 67–70 (2006).
8. Kleckner, D. & Bouwmeester, D. Sub-kelvin optical cooling of a micromechanical resonator. *Nature* **444,** 75–78 (2006).
9. Kippenberg, T. J. & Vahala, K. J. Cavity opto-mechanics. *Opt. Express* **15,** 17172–17205 (2007).
10. Favero, I. & Karrai, K. Optomechanics of deformable optical cavities. *Nature Photon.* **3,** 201–205 (2009).
11. Kippenberg, T. J. & Vahala, K. J. Cavity optomechanics: Back-action at the mesoscale. *Science* **321,** 1172–1176 (2008).
12. Chaumet, P. C. & Nieto-Vesperinas, M. Optical binding of particles with or without the presence of a flat dielectric surface. *Phys. Rev. B* **64,** 035422 (2001).
13. Nieto-Vesperinas, M., Chaumet, P. C. & Rahmani, A. Near-field photonic forces. *Phil. Trans. R. Soc. Lond. Ser. A* **362,** 719–737 (2004).
14. Rahmani, A. & Chaumet, P. C. Optical trapping near a photonic crystal. *Opt. Express* **14,** 6353–6358 (2006).
15. Povinelli, M. *et al.* High-*Q* enhancement of attractive and repulsive optical forces between coupled whispering-gallery-mode resonators. *Opt. Express* **13,** 8286–8295 (2005).
16. Povinelli, M. L. *et al.* Evanescent-wave bonding between optical waveguides. *Opt. Lett.* **30,** 3042–3044 (2005).
17. Notomi, M., Taniyama, H., Mitsugi, S. & Kuramochi, E. Optomechanical wavelength and energy conversion in high-*Q* double-layer cavities of photonic crystal slabs. *Phys. Rev. Lett.* **97,** 023903 (2006).
18. Novotny, L. & Hecht, B. *Principles of nano-optics*, Ch. 13 (Cambridge Univ. Press, 2006).
19. Rakich, P. T., Popovic, M. A. & Wang, Z. General treatment of optical forces and potentials in mechanically variable photonic systems. *Opt. Express* **17,** 18116–18135 (2009).
20. Pernice, W. H. P., Li, M. & Tang, H. X. Theoretical investigation of the transverse optical force between a silicon nanowire waveguide and a substrate. *Opt. Express* **17,** 1806–1816 (2009).
21. Vassallo, C. *Optical Waveguide Concepts* (Elsevier, 1991).
22. Riboli, F., Recati, A., Antezza, M. & Carusotto, I. Radiation induced force between two planar waveguides. *Eur. Phys. J. D* **46,** 157–164 (2008).
23. Wiederhecker, G. S. *et al.* Field enhancement within an optical fibre with a subwavelength air core. *Nature Photon.* **1,** 115–118 (2007).
24. Almeida, V. R., Xu, Q., Barrios, C. A. & Lipson, M. Guiding and confining light in void nanostructure. *Opt. Lett.* **29,** 1209–1211 (2004).
25. Li, M. *et al.* Harnessing optical forces in integrated photonic circuits. *Nature* **456,** 480–484 (2008).
26. Selvaraja, S. K. *et al.* Fabrication of photonic wire and crystal circuits in silicon-on-insulator using 193-nm optical lithography. *J. Lightwave Tech.* **27,** 4076–4083 (2009).
27. Li, M., Pernice, W. H. P. & Tang, H. X. Tunable bipolar optical interactions between guided lightwaves. *Nature Photon.* **3,** 464–468 (2009).
28. Roels, J. *et al.* Tunable optical forces between nanophotonic waveguides. *Nature Nanotech.* **4,** 510–513 (2009).
29. Kubo, R. The fluctuation-dissipation theorem. *Rep. Prog. Phys.* **29,** 255–284 (1966).
30. Rosenberg, J., Lin, Q. & Painter, O. Static and dynamic wavelength routing via the gradient optical force. *Nature Photon.* **3,** 478–483 (2009).
31. Hauss, H. A. *Waves and Fields in Optoelectronics* (Prentice Hall, 1983).
32. Little, B. E., Chu, S. T., Haus, H. A., Foresi, J. & Laine, J.-P. Microring resonator channel dropping filters. *IEEE J. Lightwave Tech.* **15,** 998–1005 (1997).
33. Eichenfield, M., Michael, C. P., Perahia, R. & Painter, O. Actuation of micro-optomechanical systems via cavity-enhanced optical dipole forces. *Nature Photon.* **1,** 416–422 (2007).
34. Pernice, W. H. P., Li, M. & Tang, H. X. Optomechanical coupling in photonic crystal supported nanomechanical waveguides. *Opt. Express* **17,** 12424–12432 (2009).
35. Anetsberger, G. *et al.* Near-field cavity optomechanics with nanomechanical oscillators. *Nature Phys.* **5,** 909–914 (2009).
36. Verbridge, S. S., Craighead, H. G. & Parpia, J. M. A megahertz nanomechanical resonator with room temperature quality factor over a million. *Appl. Phys. Lett.* **92,** 013112 (2008).
37. Ng, J., Chan, C. T., Sheng, P. & Lin, Z. Strong optical force induced by morphology-dependent resonances. *Opt. Lett.* **30,** 1956–1958 (2005).
38. Ward, J. M., Wu, Y., Minogin, V. G. & Chormaic, S. N. Trapping of a microsphere pendulum resonator in an optical potential. *Phys. Rev. A* **79,** 053839 (2009).
39. Rakich, P., Popović, M. A., Soljačić, M. & Ippen, E. P. Trapping, corralling and spectral bonding of optical resonances through optically induced potentials. *Nature Photon.* **1,** 658–665 (2007).
40. Wiederhecker, G. S., Chen, L., Gondarenko, A. & Lipson, M. Controlling photonic structures using optical forces. *Nature* **462,** 633–636 (2009).
41. Jiang, X., Lin, Q., Rosenberg, J., Vahala, K. & Painter, O. High-*Q* double-disk microcavities for cavity optomechanics. *Opt. Express* **17,** 20911–20919 (2009).
42. Gan, F. *et al.* in *Photonics in Switching* **2007**, 67–68 (IEEE, 2007).
43. Christiaens, I., Van Thourhout, D. & Baets, R. Low-power thermo-optic tuning of vertically coupled microring resonators. *Electron. Lett.* **40,** 560–561 (2004).
44. Eichenfield, M., Camacho, R., Chan, J., Vahala, K. J. & Painter, O. A picogram- and nanometre-scale photonic-crystal optomechanical cavity. *Nature* **459,** 550–555 (2009).
45. Lin, Q., Rosenberg, J., Jiang, X., Vahala, K. J. & Painter, O. Mechanical oscillation and cooling actuated by the optical gradient force. *Phys. Rev. Lett.* **103,** 103601 (2009).
46. Camacho, R. M., Chan, J., Eichenfield, M. & Painter, O. Characterization of radiation pressure and thermal effects in a nanoscale optomechanical cavity. *Opt. Express* **17,** 15726–15735 (2009).
47. Eichenfield, M., Chan, J., Camacho, R. M., Vahala, K. J. & Painter, O. Optomechanical crystals. *Nature* **462,** 78–82 (2009).
48. Yang, Y. T., Callegari, C., Feng, X. L., Ekinci, K. L. & Roukes, M. L. Zeptogram-scale nanomechanical mass sensing. *Nano Lett.* **6,** 583–586 (2006).
49. Karabacak, D., Kouh, T. & Ekinci, K. L. Analysis of optical interferometric displacement detection in nanoelectromechanical systems. *J. Appl. Phys.* **98,** 124309 (2005).
50. De Vlaminck, I. *et al.* Detection of nanomechanical motion by evanescent light wave coupling. *Appl. Phys. Lett.* **90,** 233116 (2007).
51. Li, M., Pernice, W. H. P. & Tang, H. X. Broadband all-photonic transduction of nanocantilevers. *Nature Nanotech.* **4,** 377–382 (2009).
52. Xu, Q., Manipatruni, S., Schmidt, B., Shakya, J. & Lipson, M. 12.5 Gbit/s carrier-injection-based silicon micro-ring silicon modulators. *Opt. Express* **15,** 430–436 (2007).
53. Marris-Morini, D. *et al.* Optical modulation by carrier depletion in a silicon PIN diode. *Opt. Express* **14,** 10838–10843 (2006).
54. Thompson, J. D. *et al.* Strong dispersive coupling of a high-finesse cavity to a micromechanical membrane. *Nature* **452,** 72–75 (2008).
55. Bhattacharya, M., Uys, H. & Meystre, P. Optomechanical trapping and cooling of partially reflective mirrors. *Phys. Rev. A* **77,** 033819 (2008).